

¹ **Differential response of a tree-killing bark beetle to forest structure
2 and composition across a gradient of climatic water deficit**

³ Michael J. Koontz^{1,2,3*}, Andrew M. Latimer^{1,2}, Leif A. Mortenson⁴, Christopher J. Fettig⁵, Malcolm P.
⁴ North^{1,2,6}

⁵ ¹Graduate Group in Ecology, University of California, Davis, CA, USA

⁶ ²Department of Plant Sciences, University of California, Davis, CA, USA

⁷ ³Earth Lab, University of Colorado-Boulder; Boulder, CO, USA

⁸ ⁴USDA Forest Service, Pacific Southwest Research Station, Placerville, CA, USA

⁹ ⁵USDA Forest Service, Pacific Southwest Research Station, Davis, CA, USA

¹⁰ ⁶USDA Forest Service, Pacific Southwest Research Station, Mammoth Lakes, CA, USA

¹¹ *Correspondence: michael.koontz@colorado.edu

¹² *Keywords:* bark beetles, forest structure, drones, climatic water deficit, Sierra Nevada, California, disturbance,
¹³ structure from motion, *Dendroctonus brevicomis*, *Pinus ponderosa*, threshold dynamics

¹⁴ *Abstract word count:* 336

¹⁵ *Overall .docx word count:* 11096 *Main text word count:* 6967 (Intro: 1249; Methods: 3176
¹⁶ (679+647+1540+310); Results: 344 (41+102+201); Discussion: 2198)

¹⁷ *Text boxes word count:* 0

¹⁸ Date report generated: September 17, 2019

¹⁹ **Abstract**

²⁰ 1. The Californian hot drought of 2012 to 2015 created favorable conditions for unprecedented ponderosa
²¹ pine (*Pinus ponderosa*) mortality in the Sierra Nevada mountain range, largely attributable to the
²² western pine beetle (WPB; *Dendroctonus brevicomis*). Climate conditions and forest density may
²³ interact to affect tree mortality, but density is a coarse gauge of forest structure that can affect WPB
²⁴ behavior in a number of ways. Measuring broad-scale climate conditions simultaneously with local forest
²⁵ composition and structure— the spatial distribution and size of trees— will refine our understanding of
²⁶ how these variables interact, but is generally expensive and/or labor-intensive.

²⁷ 2. We use drone surveys over a network of 160 field plots along a 350km and 1000m elevation gradient in
²⁸ western slope Sierra Nevada ponderosa pine/mixed-conifer forests and Structure from Motion processing
²⁹ to segment and classify more than 450,000 trees over 9km² of forest with WPB-induced tree mortality.

30 We modeled the probability of ponderosa pine mortality as a function of forest structure and composition
31 variables and their interaction with site-level climatic water deficit, accounting for spatial covariance
32 using exact Gaussian processes.

- 33 3. Greater host density strongly increased the probability of host mortality, while greater overall density
34 decreased mortality. Further, we found a strong interaction between host size and climatic water deficit
35 such that larger trees increased the probability of host mortality at hot/dry sites, but smaller trees
36 tended to drive mortality in cool/wet sites.
- 37 4. Our results demonstrate a variable response of the WPB to local forest structure and composition
38 across an environmental gradient during the same hot drought, which may indicate forest sites were in
39 different stages of disturbance (from “endemic” to “outbreak”) depending on their regional climate.
40 Management interventions that reduce host density may decrease the probability of tree mortality
41 attributed to western pine beetles in the future, and our results suggest that focusing these treatments
42 on areas that are most likely to exceed feedback thresholds (i.e., hot/dry sites with many available
43 hosts) will have the best chance of increasing tree survivorship, specifically of larger trees.

44 **Introduction**

45 Bark beetles dealt the final blow to many of the nearly 150 million trees killed in the California hot drought
46 of 2012 to 2015 and its aftermath (USDAFS 2019). A harbinger of climate change effects to come, record
47 high temperatures exacerbated the drought (Griffin and Anchukaitis 2014), which increased water stress on
48 trees (Asner et al. 2016), making them more susceptible to colonization by bark beetles (Fettig 2012, Kolb et
49 al. 2016). Further, a century of fire suppression policy has enabled forests to grow into dense stands, which
50 also makes them more vulnerable to bark beetles (Fettig 2012). This combination of environmental conditions
51 and forest structural characteristics led to tree mortality events of unprecedented size in the driest, densest
52 forests across the state (Young et al. 2017). The mechanisms underlying the link between tree susceptibility
53 to colonization by insects and hot, dry conditions are often directly attributed to tree physiology (Bentz et al.
54 2010), while the link to forest density is multifaceted (Fettig 2012). Because forest density is a coarse metric
55 of the forest features to which bark beetles respond (Raffa et al. 2008), our understanding of the connection
56 between forest density and insect disturbance severity could be enhanced with more finely-resolved measures
57 of forest structure as well as explicit consideration of species composition (Stephenson et al. 2019, Fettig et al.
58 2019). Finally, the challenge of simultaneously measuring the effects of both local-scale forest features (such
59 as structure and composition) and broad-scale environmental conditions on forest insect disturbance leaves
60 their interaction effect relatively underexplored (Seidl et al. 2016, Stephenson et al. 2019, Fettig et al. 2019).

61 The ponderosa pine/mixed-conifer forests in California's Sierra Nevada region are characterized by regular
62 bark beetle disturbances, primarily by the influence of western pine beetle (*Dendroctonus brevicomis*; WPB)
63 on its host ponderosa pine (*Pinus ponderosa*) (Fettig 2016). The WPB is a "primary" bark beetle— its
64 reproductive success is contingent upon host tree mortality, which itself requires enough beetles to "mass
65 attack" the host tree and overwhelm its defenses (Raffa and Berryman 1983). This Allee effect creates a
66 strong coupling between beetle selection behavior of host trees and host tree susceptibility to colonization
67 (Raffa and Berryman 1983, Logan et al. 1998). A key defense mechanism of trees to bark beetle attack is to
68 flood beetle bore holes with resin, which physically expels beetles and may interrupt beetle communication
69 (Franceschi et al. 2005, Raffa et al. 2015). Under normal conditions, weakened trees with compromised
70 defenses are the most susceptible to colonization and will be the main targets of primary bark beetles like
71 the western pine beetle (Bentz et al. 2010, Raffa et al. 2015). Under severe water stress, many trees no
72 longer have the resources available to mount a defense (Kolb et al. 2016) and thus prolonged drought can
73 often trigger increased bark beetle-induced tree mortality as average tree vigor declines (Bentz et al. 2010).
74 As local population density of beetles increases due to successful reproduction within spatially-aggregated
75 weakened trees, as might occur during drought, mass attacks grow in size and become capable of overwhelming
76 formidable tree defenses such that even healthy trees may be susceptible to colonization and mortality (Bentz
77 et al. 2010, Raffa et al. 2015). Thus, water stress can be a key determinant of whether individual trees are
78 susceptible to bark beetles under many conditions, and this environmental condition may interact with beetle
79 population dynamics to drive tree susceptibility under extreme conditions (Bentz et al. 2010, Stephenson et
80 al. 2019).

81 Western pine beetle activity is strongly influenced by forest structure—the spatial distribution and size of
82 trees—and tree species composition. Taking forest structure alone, high-density forests are more prone to
83 bark beetle-induced tree mortality (Fettig 2012) which may arise as greater competition for water resources
84 amongst crowded trees and thus average tree resistance is lower (Hayes et al. 2009), or because smaller gaps
85 between trees protect pheromone plumes from dissipation by the wind and thus enhance intraspecific beetle
86 communication (Thistle et al. 2004). Tree size is another aspect of forest structure that affects bark beetle
87 host selection behavior with smaller trees tending to have lower capacity for resisting attack, and larger
88 trees being a more desirable target on account of their thicker phloem providing greater nutritional content
89 (Chubaty et al. 2009, Graf et al. 2012). Taking forest composition alone, WPB activity in the Sierra Nevada
90 range of California is necessarily tied to the regional distribution of its exclusive host, ponderosa pine (Fettig
91 2016). Colonization by primary bark beetles can also depend on the relative frequencies of tree species in a
92 more local area, akin to reduced oligophagous insect herbivory in forests comprising taxonomically distinct

93 tree species compared to monocultures (Jactel and Brockerhoff 2007). The interaction between forest structure
94 and composition also drives WPB activity. For instance, high density forests with high host availability may
95 experience greater beetle-induced tree mortality because dispersal distances between potential host trees are
96 shorter and facilitate successful colonization (Miller and Keen 1960, Berryman 1982, Fettig et al. 2007) or
97 because high host availability reduces the chance of individual beetles wasting their limited resources flying
98 to and landing on a non-host tree (Moeck et al. 1981, Evenden et al. 2014). Stand-scale measures of forest
99 structure and composition thus paint a fundamentally limited picture of the mechanisms by which these
100 forest characteristics affect bark beetle disturbance, but finer-grain information explicitly recognizing tree
101 size, species, and local tree density should more appropriately capture the ecological processes underlying
102 insect-induced tree mortality. Additionally, considering the effects of local forest structure and composition
103 with the effects of environmental conditions may help refine our understanding of tree mortality patterns in
104 widespread events such as during the recent California hot drought.

105 The vast spatial extent of tree mortality in the 2012 to 2015 California hot drought challenges our ability to
106 simultaneously consider how broad-scale environmental conditions may interact with local forest structure
107 and composition to affect the dynamic between bark beetle selection and colonization of host trees, and host
108 tree susceptibility to attack (Anderegg et al. 2015, Stephenson et al. 2019). Measuring local forest structure
109 generally requires expensive instrumentation (Kane et al. 2014, Asner et al. 2016) or labor-intensive field
110 surveys (Larson and Churchill 2012, Stephenson et al. 2019, Fettig et al. 2019), which constrains survey
111 extent and frequency. Small, unhumanned aerial systems (sUAS) enable relatively fast and cheap remote
112 imaging over dozens of hectares of forest, which can be used to measure complex forest structure at the
113 individual tree scale (Morris et al. 2017, Shiklomanov et al. 2019). Distributing such surveys across an
114 environmental gradient can overcome the data acquisition challenge inherent in investigating phenomena
115 with both a strong local- and a strong broad-scale component.

116 We used ultra-high resolution, sUAS-derived remote sensing data over a network of 32 sites in Sierra Nevada
117 ponderosa pine/mixed-conifer forests spanning 1000m of elevation and 350km of latitude (see Fettig et al.
118 (2019)) and covering a total of 9km² to ask how broad-scale environmental conditions interacted with local,
119 complex forest structure to affect the probability of tree mortality during the cumulative tree mortality event
120 of 2012 to 2018. We asked:

- 121 1. How does host tree density and average host tree size affect WPB-induced tree mortality?
- 122 2. How does the density of all tree species (hereafter “overall density”) and average tree size of all species
123 (hereafter “overall size”) affect WPB-induced tree mortality?

- 124 3. How does environmentally-driven tree moisture stress affect WPB-induced tree mortality?
- 125 4. Do the effects of forest structure, forest composition, and environmental condition interact to influence
- 126 WPB-induced tree mortality?

127 **Methods**

128 **Study system**

129 We built our study coincident with 160 vegetation/forest insect monitoring plots at 32 sites established
130 between 2016 and 2017 by Fettig et al. (2019) (Figure 1). The study sites were chosen to reflect typical
131 west-side Sierra Nevada yellow pine/mixed-conifer forests and were dominated by ponderosa pine trees, *Pinus*
132 *ponderosa* (Fettig et al. 2019). These established plots were located in WPB-attacked, yellow pine/mixed-
133 conifer forests across the Eldorado, Stanislaus, Sierra and Sequoia National Forests and were stratified by
134 elevation (914-1219 m [3000-4000 ft], 1219-1524 m [4000-5000 ft], 1524-1829 m [5000-6000 ft] above sea level).

135 In the Sequoia National Forest, the southernmost National Forest in our study, plots were stratified with the
136 lowest elevation band between 1219 and 1524 m (4000-5000 ft) and extended to an upper elevation band of
137 1829-2134 m (6000-7000 ft) to capture a more similar forest community composition as at the more northern
138 National Forests. The sites have variable forest structure and plot locations were selected in areas with >35%
139 ponderosa pine basal area and >10% ponderosa pine mortality. At each site, five 0.041 ha circular plots were
140 installed along transects with 80 to 200m between plots. In the field, Fettig et al. (2019) mapped all stem
141 locations relative to the center of each plot using azimuth/distance measurements. Tree identity to species,
142 tree height, and diameter at breast height (DBH) were recorded if DBH was greater than 6.35cm. Year of
143 mortality was estimated based on needle color and retention, if it wasn't directly observed during site visits.
144 A small section of bark (approximately 625 cm²) on both north and south aspects was removed from dead
145 trees to determine if bark beetle galleries were present. The shape, distribution, and orientation of galleries
146 are commonly used to distinguish among bark beetle species (Fettig 2016). In some cases, deceased bark
147 beetles were present beneath the bark to supplement identifications based on gallery formation. During the
148 spring and early summer of 2018, all field plots were revisited to assess whether dead trees had fallen (Fettig
149 et al. 2019).

150 In the typical life cycle of western pine beetles, female WPB initiate host colonization by tunneling through
151 the outer bark and into the phloem and outer xylem where they rupture resin canals. As a result, oleoresin
152 exudes and collects on the bark surface, as is commonly observed with other bark beetle species. During the
153 early stages of attack, females release an aggregation pheromone component which, in combination with host

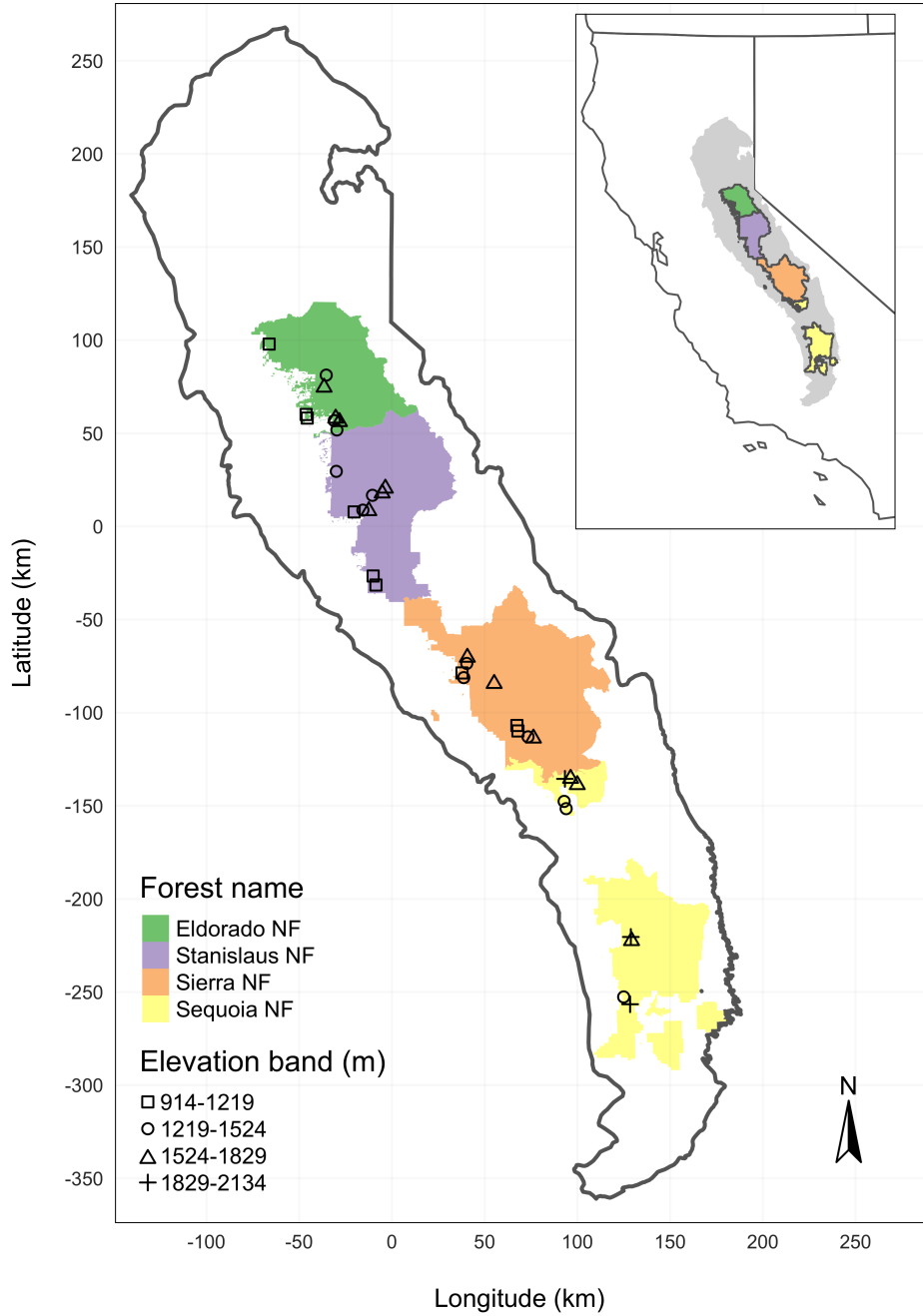


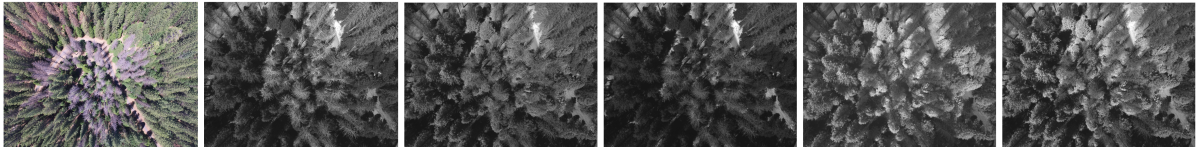
Figure 1: The network of field plots spanned a 350 km latitudinal gradient from the Eldorado National Forest in the north to the Sequoia National Forest in the south. Plots were stratified by three elevation bands in each forest, with the plots in the Sequoia National Forest (the southern-most National Forest) occupying elevation bands 305m above the three bands in the other National Forests in order to capture a similar community composition.

monoterpenes released from pitch tubes, is attractive to conspecifics (Bedard et al. 1969). An antiaggregation pheromone component is produced during latter stages of host colonization by several pathways, and is thought to reduce intraspecific competition by altering adult behavior to minimize overcrowding of developing brood within the host (Byers and Wood 1980). Volatiles from several nonhosts sympatric with ponderosa pine have been demonstrated to inhibit attraction of WPB (Shepherd et al. 2007, Fettig and Hilszczański 2015). In California, the WPB can have 2-3 generations in a single year and can often out-compete its congener, the mountain pine beetle, *Dendroctonus ponderosa* (MPB), for the ponderosa pine host especially in larger trees (Miller and Keen 1960, Fettig 2016).

Aerial data collection and processing

Nadir-facing imagery was captured using a gimbal-stabilized DJI Zenmuse X3 broad-band red/green/blue (RGB) camera (DJI 2015a) and a fixed-mounted Micasense Rededge3 multispectral camera with five narrow bands (Micasense 2015) on a DJI Matrice 100 aircraft (DJI 2015b). Imagery was captured from both cameras along preprogrammed aerial transects over ~40 hectares surrounding each of the 36 sites (each of these containing five field plots) and was processed in a series of steps to yield local forest structure and composition data suitable for our statistical analysis. Following the call by Wyngaard et al. (2019), we establish “data product levels” to reflect the image processing pipeline from raw imagery (Level 0) to calibrated, fine-scale forest structure and composition information on regular grids (Level 4), with each new data level derived from levels below it. Here, we outline the steps in the processing and calibration pipeline visualized in Figure 2, and include additional details in the Supplemental Methods.

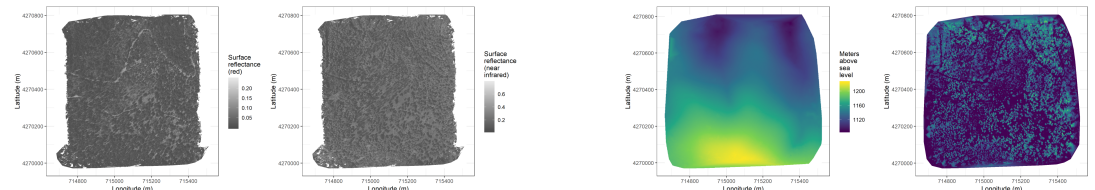
Level 0: raw data from sensors



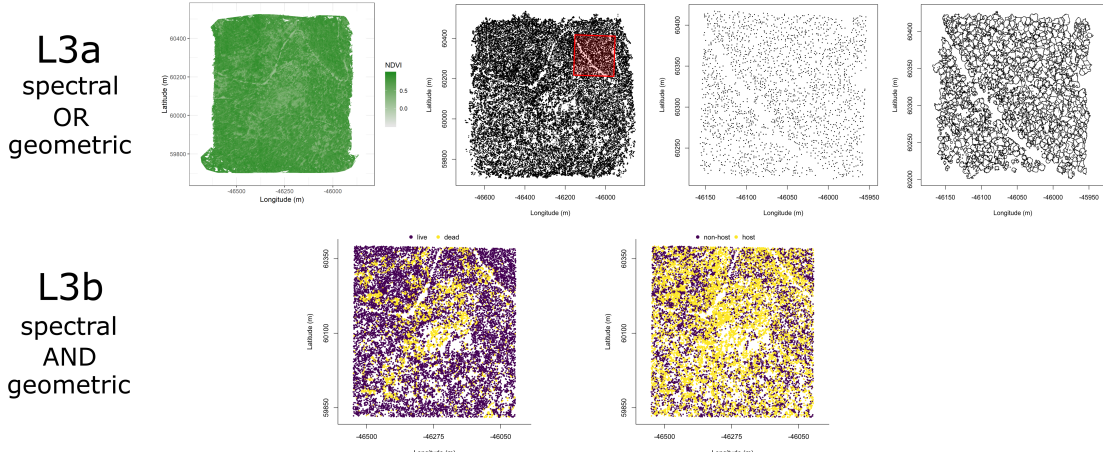
Level 1: basic outputs from photogrammetric processing



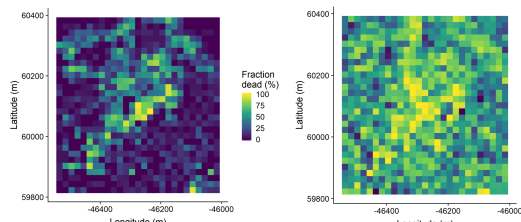
Level 2: corrected outputs from photogrammetric processing



Level 3: domain-specific information extraction



Level 4: aggregations to regular grids



174 Figure 2. Schematic of the data processing workflow for a single site with each new data product level derived
175 from data at lower levels.

176 Level 0 represents raw data from the sensors. From left to right: example broad-band RGB photo from
177 DJI Zenmuse X3 camera, example blue photo from Rededge3 (centered on 475nm), example green photo
178 from Rededge3 (centered on 560nm), example red photo from Rededge3 (centered on 668nm), example near
179 infrared photo from Rededge3 (centered on 840nm), and example red edge photo from Rededge3 (centered on
180 717nm).

181 Level 1 represents basic outputs from the photogrammetric workflow, in this case implemented with
182 Pix4Dmapper. From left to right: a dense point cloud visualized in CloudCompare (<https://www.danielgm.net/cc/>), an orthophoto generated from the RGB camera, and a digital surface model representing the
183 altitude above sea level (ground height + vegetation height) for every cell.
184

185 Level 2 represents outputs from photogrammetric processing that have been corrected radiometrically or
186 geometrically. From left to right: a radiometrically-corrected surface reflectance map of the red narrow band
187 from the Rededge3 camera, a radiometrically-corrected surface reflectance map of the near infrared narrow
188 band from the Rededge3 camera, a rasterized version of the digital terrain model derived by a geometric
189 correction of the dense point cloud, and a canopy height model derived by subtracting the terrain height
190 from the digital surface model.

191 Level 3 represents domain-specific information extraction from Level 2 products and is divided into two
192 sub-levels. Level 3a products are derived using only spectral or only geometric data. From left to right: a
193 reflectance map of Normalized Difference Vegetation Index (NDVI; Rouse et al. (1973)) derived using the red
194 and near infrared Level 2 reflectance products, a map of points representing detected trees from the canopy
195 height model with a red polygon highlighting the area presented in more detail for the next two images, a
196 close-up of points representing detected trees, and a close-up of polygons representing segmented tree crowns.
197 Level 3b products are derived using both spectral and geometric data. From left to right: a map of the point
198 locations of detected trees that have been classified as alive or dead based on the pixel values within each
199 segmented tree crown and a map of the point locations of detected trees classified to WPB host/non-host
200 using the same spectral information. Note that our study relies on the generation of Level 3a products in
201 order to combine them and create Level 3b products, but this need not be the case. For instance, deep
202 learning/neural net methods may be able to use both the spectral and geometric information from Level 2
203 simultaneously to locate and classify trees in a scene and directly generate Level 3b products without a need
204 to first generate the Level 3a products shown in this schematic.

205 Level 4 represents aggregations of Level 3 products to regular grids which might better reflect the grain size
206 of the data for which we have the best calibration and thus the most confidence or which might provide
207 new information not possible at an individual-tree level (e.g., average distance between trees in a small
208 neighborhood) From left to right: aggregation of live/dead classified trees as fraction of dead trees in a 20 x
209 20-m cell and aggregation of host/non-host classified trees as fraction of hosts in a 20 x 20-m cell. In our
210 case, the 20 x 20-m aggregation produces a grid cell with an area of 400m², which most closely matches the
211 404m² area of the ground-based vegetation plots whose data we used in an aggregated form to calibrate our
212 derivation of Level 3 products.

213 **Level 0: Raw data from sensors**

214 Raw data comprised approximately 1900 images per camera lens (one broad-band RGB lens and five narrow-
215 band multispectral lenses) for each of the 32 sites (Figure 2; Level 0). Prior to the aerial survey, two strips
216 of bright orange drop cloth (~100 cm x 15 cm) were positioned as an “X” over the permanent monuments
217 marking the center of the 5 field plots from Fettig et al. (2019) (see Supplemental Figures).

218 We preprogrammed north-south aerial transects using Map Pilot for DJI on iOS flight software (Drones-
219 MadeEasy 2018) at an altitude of 120 m above ground level (with “ground” defined using a 1-arc-second
220 digital elevation model (Farr et al. 2007)). The resulting ground sampling distance was approximately 5
221 cm/px for the Zenmuse X3 RGB camera and approximately 8 cm/px for the Rededge3 multispectral camera.
222 We used 91.6% image overlap (both forward and side) at the ground for the Zenmuse X3 RGB camera and
223 83.9% overlap (forward and side) for the Rededge3 multispectral camera.

224 **Level 1: Basic outputs from photogrammetric processing**

225 We used structure from motion (SfM) photogrammetry implemented in Pix4Dmapper Cloud (www.pix4d.com)
226 to generate dense point clouds (Figure 2; Level 1, left), orthophotos (Figure 2; Level 1, center), and digital
227 surface models (Figure 2; Level 1, right) for each field site (Frey et al. 2018). For 29 sites, we processed the
228 Rededge3 multispectral imagery alone to generate these products. For three sites, we processed the RGB and
229 the multispectral imagery together to enhance the point density of the dense point cloud. All SfM projects
230 resulted in a single processing “block,” indicating that all images in the project were optimized and processed
231 together. The dense point cloud represents x, y, and z coordinates as well as the color of millions of points
232 per site. The orthophoto represents a radiometrically uncalibrated, top-down view of the survey site that
233 preserves the relative x/y positions of objects in the scene. The digital surface model is a rasterized version
234 of the dense point cloud that shows the altitude above sea level for each pixel in the scene at the ground

235 sampling distance of the camera that generated the Level 0 data.

236 **Level 2: Corrected outputs from photogrammetric processing**

237 **Radiometric corrections**

238 A radiometrically-corrected reflectance map (Figure 2; Level 2, left two figures; i.e., a corrected version of the
239 Level 1 orthophoto) was generated using the Pix4D software by incorporating incoming light conditions for
240 each narrow band of the Rededge3 camera (captured simultaneously with the Rededge3 camera using an
241 integrated downwelling light sensor) as well as a pre-flight image of a calibration panel of known reflectance
242 (see Supplemental Methods for camera and calibration panel details).

243 **Geometric corrections**

244 We implemented a geometric correction to the Level 1 dense point cloud and digital surface model by
245 normalizing these data for the terrain underneath the vegetation. We generated the digital terrain model
246 representing the ground underneath the vegetation at 1 meter resolution (Figure 2; Level 2, third image)
247 by classifying each survey area's dense point cloud into "ground" and "non-ground" points using a cloth
248 simulation filter algorithm (Zhang et al. 2016) implemented in the `lidR` (Roussel et al. 2019) package and
249 rasterizing the ground points using the `raster` package (Hijmans et al. 2019). We generated a canopy height
250 model (Figure 2; Level 2, fourth image) by subtracting the digital terrain model from the digital surface
251 model.

252 **Level 3: Domain-specific information extraction**

253 **Level 3a: Data derived from spectral OR geometric Level 2 product**

254 Using just the spectral information from the radiometrically-corrected reflectance maps, we calculated several
255 vegetation indices including the normalized difference vegetation index (NDVI; Rouse et al. (1973); Figure
256 2; Level 3a, first image), the normalized difference red edge (NDRE; Gitelson and Merzlyak (1994)), the
257 red-green index (RGI; Coops et al. (2006)), the red edge chlorophyll index ($CI_{red\ edge}$; Clevers and Gitelson
258 (2013)), and the green chlorophyll index (CI_{green} ; Clevers and Gitelson (2013)).

Table 1: Algorithm name, number of parameter sets tested for each algorithm, and references.

Algorithm	Parameter sets tested	Reference(s)
li2012	131	Li et al. (2012); Jakubowski et al. (2013); Shin et al. (2018)

Algorithm	Parameter sets tested	Reference(s)
lmfx	30	Roussel (2019)
localMaxima	6	Roussel et al. (2019)
multichm	1	Eysn et al. (2015)
ptrees	3	Vega et al. (2014)
vwf	3	Plowright (2018)
watershed	3	Pau et al. (2010)

259 Using just the geometric information from the canopy height model or terrain-normalized dense point cloud,
 260 we generated maps of detected trees (Figure 2; Level 3a, second and third images) by testing a total of 7
 261 automatic tree detection algorithms and a total of 177 parameter sets (Table 1). We converted the height
 262 of each tree determined using the Level 2 canopy height model to its diameter at breast height, 1.37m
 263 (DBH). We used the field plot data to assess each tree detection algorithm/parameter set by converting the
 264 distance-from-center and azimuth measurements of the trees in the field plots to x-y positions relative to the
 265 field plot centers distinguishable in the Level 2 reflectance maps as the orange fabric X's that we laid out
 266 prior to each flight. In the reflectance maps, we located 110 out of 160 field plot centers while some plot
 267 centers were obscured due to dense interlocking tree crowns or because a plot center was located directly
 268 under a single tree crown. For each of the 110 field plots with identifiable plot centers– the “validation field
 269 plots”, we calculated 7 forest structure metrics using the ground data collected by Fettig et al. (2019): total
 270 number of trees, number of trees greater than 15 meters, mean height of trees, 25th percentile tree height,
 271 75th percentile tree height, mean distance to nearest tree neighbor, and mean distance to second nearest
 272 neighbor. For each tree detection algorithm and parameter set described above, we calculated the same set of
 273 7 structure metrics within the footprint of the validation field plots. We calculated the Pearson’s correlation
 274 and root mean square error (RMSE) between the ground data and the aerial data for each of the 7 structure
 275 metrics for each of the 177 automatic tree detection algorithms/parameter sets. For each algorithm and
 276 parameter set, we calculated its performance relative to other algorithms as whether its Pearson’s correlation
 277 was within 5% of the highest Pearson’s correlation as well as whether its RMSE was within 5% of the lowest
 278 RMSE. We summed the number of forest structure metrics for which it reached these 5% thresholds for
 279 each algorithm/parameter set. For automatically detecting trees across the whole study, we selected the
 280 algorithm/parameter set that performed well across the most number of forest metrics (see Results).

281 We delineated individual tree crowns (Figure 2; Level 3a, fourth image) with a marker controlled watershed

282 segmentation algorithm (Meyer and Beucher 1990) implemented in the **ForestTools** package (Plowright
283 2018) using the detected treetops as markers. If the automatic segmentation algorithm failed to generate
284 a crown segment for a detected tree (e.g., often snags with a very small crown footprint), a circular crown
285 was generated with a radius of 0.5 meters. If the segmentation generated multiple polygons for a single
286 detected tree, only the polygon containing the detected tree was retained. Because image overlap decreases
287 near the edges of the overall flight path and reduces the quality of the SfM processing in those areas, we
288 excluded segmented crowns within 35 m of the edge of the survey area. Given the narrower field of view of
289 the Rededge3 multispectral camera versus the X3 RGB camera whose optical parameters were used to define
290 the ~40 hectare survey area around each site, as well as the 35 m additional buffering, the survey area at
291 each site was ~30 ha (see Supplemental Methods).

292 **Level 3b: Data derived from spectral AND geometric information**

293 We overlaid the segmented crowns on the reflectance maps from 20 sites spanning the latitudinal and elevation
294 gradient in the study. Using QGIS (<https://qgis.org/en/site/>), we hand classified 564 trees as live/dead
295 (Figure 3) and as one of 5 dominant species in the study area (*Pinus ponderosa*, *Pinus lambertiana*, *Abies*
296 *concolor*, *Calocedrus decurrens*, or *Quercus kelloggii*) using the mapped ground data as a guide. Each tree was
297 further classified as “host” for ponderosa pine or “non-host” for all other species (Fettig 2016). We extracted
298 all the pixel values within each segmented crown polygon from the five, Level 2 orthorectified reflectance
299 maps (one per narrow band on the Rededge3 camera) as well as from the five, Level 3a vegetation index
300 maps using the **velox** package (Hunziker 2017). For each crown polygon, we calculated the mean value of
301 the extracted Level 2 and Level 3a pixels and used them as ten independent variables in a five-fold cross
302 validated boosted logistic regression model to predict whether the hand classified trees were alive or dead.
303 For just the living trees, we similarly used all 10 mean reflectance values per crown polygon to predict tree
304 species using a five-fold cross validated regularized discriminant analysis. The boosted logistic regression and
305 regularized discriminant analysis were implemented using the **caret** package in R (Kuhn 2008). Finally, we
306 used these models to classify all tree crowns in the data set as alive or dead (Figure 2; Level 3b, first image)
307 as well as the species of living trees (Figure 2; Level 3b, second image).

308 Using the tree height and DBH field data from Fettig et al. (2019), we fit a simple linear regression to
309 predict DBH from height for each of the five dominant species in the study area. We used these species-
310 specific allometric relationships between field-measured tree height and DBH to estimate the DBH of each
311 model-classified tree given its species and height.

312 **Level 4: Aggregations to regular grids**

313 We rasterized the forest structure and composition data at a spatial resolution similar to that of the field
314 plots to better match the grain size at which we validated the automatic tree detection algorithms. In each
315 raster cell, we calculated: number of live trees, number of dead trees, number of ponderosa pine trees, total
316 number of trees (of all species, including ponderosa pine). From these values, we calculated the fraction of
317 dead trees per cell (Figure 2; Level 4, first image) and the fraction of host trees per cell (Figure 2; Level
318 4, second image). We converted the count of ponderosa pine trees and the total tree count to a density
319 measurement of trees per hectare (tpha) by multiplying the counts in each 20 x 20-m cell by 25 to create a
320 “host density” and an “overall density” variable per cell. Finally, we then calculated a separate quadratic
321 mean diameter (QMD) for ponderosa pine and all trees of any species for each 20 x 20-m cell as the square
322 root of the average squared diameter of trees (ponderosa or all) within the cell.

323 **Note on assumptions about dead trees**

324 For the purposes of this study, we assumed that all dead trees were ponderosa pine and thus hosts colonized
325 by WPB. This is a reasonably good assumption for our study area; for example, Fettig et al. (2019) found
326 that 73.4% of dead trees in their coincident field plots were ponderosa pine. Mortality was concentrated in
327 the larger-diameter classes and attributed primarily to WPB (see Fettig et al. (2019), Figure 5). The species
328 contributing to the next highest proportion of dead trees was incense cedar which represented 18.72% of the
329 dead trees in the field plots. While the detected mortality is most likely to be ponderosa pine, it is critical to
330 interpret our results with this known limitation in mind.

331 **Environmental data**

332 We used climatic water deficit (CWD) (Stephenson 1998) from the 1981-2010 mean value of the basin
333 characterization model (Flint et al. 2013) as an integrated measure of temperature and moisture conditions
334 for each of the 32 sites. Higher values of CWD correspond to hotter, drier conditions and lower values
335 correspond to cooler, wetter conditions. CWD has been shown to correlate well with broad patterns of tree
336 mortality in the Sierra Nevada (Young et al. 2017) as well as bark beetle-induced tree mortality (Millar et al.
337 2012). We converted the CWD value for each site into a z-score representing that site’s deviation from the
338 mean CWD across the climatic range of Sierra Nevada ponderosa pine as determined from 179 herbarium
339 records described in Baldwin et al. (2017). Thus, a CWD z-score of 1 would indicate that the CWD at that
340 site is one standard deviation hotter/drier than the mean CWD across all geolocated herbarium records for
341 ponderosa pine in the Sierra Nevada.

³⁴² **Statistical model**

³⁴³ We used a generalized linear model with a zero-inflated binomial response and a logit link to predict the
³⁴⁴ probability of ponderosa pine mortality within each 20 x 20-m cell as a function of the crossed effects of
³⁴⁵ ponderosa pine QMD and density added to the crossed effect of QMD and density of trees of all species in
³⁴⁶ each cell (hereafter “overall QMD” and “overall density”), as well as the interaction of each summand with
³⁴⁷ climatic water deficit at each site.

³⁴⁸ To measure and account for spatial autocorrelation of the bark beetle behavioral processes underlying
³⁴⁹ ponderosa pine mortality, we subsampled the data at each site to a random selection of 200, 20 x 20-m
³⁵⁰ cells representing approximately 27.5% of the surveyed area. Additionally with these subsampled data, we
³⁵¹ included a separate exact Gaussian process term per site of the interaction between the x- and y-position of
³⁵² each cell using the `gp()` function in the `brms` package (Bürkner 2017). The Gaussian process estimates the
³⁵³ spatial covariance in the response variable (log-odds of ponderosa pine mortality) jointly with the effects of
³⁵⁴ the other covariates.

$$y_{i,j} \sim \begin{cases} 0, & p \\ Binom(n_i, \pi_i), & 1 - p \end{cases}$$

$$\begin{aligned} logit(\pi_i) = & \beta_0 + \\ & \beta_1 X_{cwd,j} + \\ & \beta_1 X_{cwd,j} (\beta_2 X_{pipoQMD,i} + \beta_3 X_{pipoDensity,i} + \beta_4 X_{pipoQMD,i} X_{pipoDensity,i}) + \\ & \beta_1 X_{cwd,j} (\beta_5 X_{overallQMD,i} + \beta_6 X_{overallDensity,i} + \beta_7 X_{overallQMD,i} X_{overallDensity,i}) + \\ & \mathcal{GP}_j(x_i, y_i) \end{aligned}$$

³⁵⁵ Where y_i is the number of dead trees in cell i , n_i is the sum of the dead trees (assumed to be ponderosa pine)
³⁵⁶ and live ponderosa pine trees in cell i , π_i is the probability of ponderosa pine tree mortality in cell i , p is the
³⁵⁷ probability of there being zero dead trees in a cell arising as a result of an unmodeled process, $X_{cwd,j}$ is the
³⁵⁸ z-score of climatic water deficit for site j , $X_{pipoQMD,i}$ is the scaled quadratic mean diameter of ponderosa
³⁵⁹ pine in cell i , $X_{pipoDensity,i}$ is the scaled density of ponderosa pine trees in cell i , $X_{overallQMD,i}$ is the scaled
³⁶⁰ quadratic mean diameter of all trees in cell i , $X_{overallDensity,i}$ is the scaled density of all trees in cell i , x_i
³⁶¹ and y_i are the x- and y- coordinates of the centroid of the cell in an EPSG3310 coordinate reference system,
³⁶² and \mathcal{GP}_j represents the exact Gaussian process describing the spatial covariance between cells at site j .

³⁶³ We used 4 chains with 2000 iterations each (1000 warmup, 1000 samples), and confirmed chain convergence

364 by ensuring all `Rhat` values were less than 1.1 (Brooks and Gelman 1998). We used posterior predictive
365 checks to visually confirm model performance by overlaying the density curves of the predicted number of
366 dead trees per cell over the observed number (Gabry et al. 2019). For the posterior predictive checks, we
367 used 50 random samples from the model fit to generate 50 density curves and ensured curves were centered
368 on the observed distribution, paying special attention to model performance at capturing counts of zero.

369 **Software and data availability**

370 All data are available via the Open Science Framework. Statistical analyses were performed using the `brms`
371 packages. With the exception of the SfM software (Pix4Dmapper Cloud) and the GIS software QGIS, all
372 data carpentry and analyses were performed using R (R Core Team 2018).

373 **Results**

374 **Tree detection algorithm performance**

375 We found that the experimental `lmfx` algorithm with parameter values of `dist2d = 1` and `ws = 2.5` (Roussel
376 et al. 2019) performed the best across 7 measures of forest structure as measured by Pearson's correlation
377 with ground data (Table 2).

Table 2: Correlation and differences between the best performing tree detection algorithm (`lmfx` with `dist2d = 1` and `ws = 2.5`) and the ground data. An asterisk next to the correlation or RMSE indicates that this value was within 5% of the value of the best-performing algorithm/parameter set. Ground mean represents the mean value of the forest metric across the 110 field plots that were visible from the sUAS-derived imagery. The median error is calculated as the median of the differences between the air and ground values for the 110 visible plots. Thus, a positive number indicates an overestimate by the sUAS workflow and a negative number indicates an underestimate.

Forest structure metric	Ground mean	Correlation with ground	RMSE	Median error
total tree count	19	0.67*	8.68*	2
count of trees > 15m	9.9	0.43	7.38	0
distance to 1st neighbor (m)	2.8	0.55*	1.16*	0.26
distance to 2nd neighbor (m)	4.3	0.61*	1.70*	0.12
height (m); 25th percentile	12	0.16	8.46	-1.2
height (m); mean	18	0.29	7.81*	-2.3
height (m); 75th percentile	25	0.35	10.33*	-4

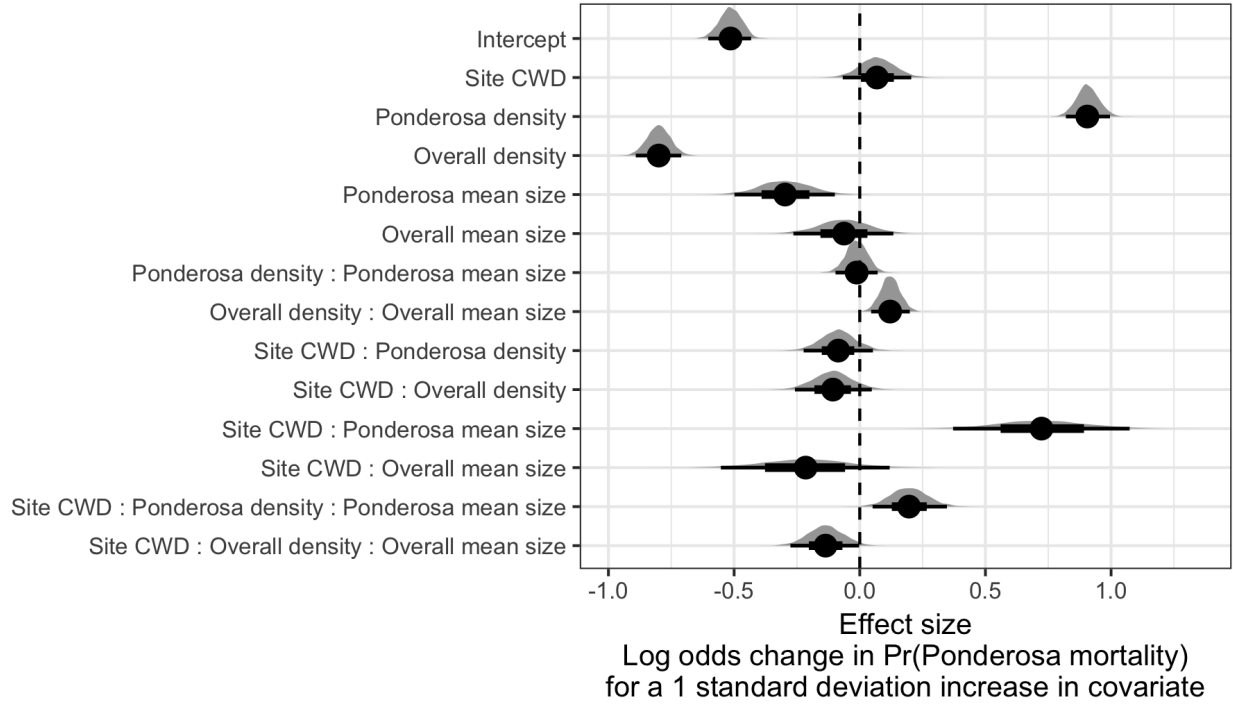


Figure 4: Posterior distributions of effect size from zero-inflated binomial model predicting the probability of ponderosa pine mortality in a 20 x 20-m cell given forest structure characteristics of host trees and all trees within the cell, as well as a site-level climatic water deficit. The gray density distribution for each model covariate represents the density of the posterior distribution, the point underneath each density curve represents the median of the estimate, the bold interval surrounding the point estimate represents the 66% credible interval, and the thin interval surrounding the point estimate represents the 95% credible interval.

378 Classification accuracy for live/dead and host/non-host

379 The accuracy of live/dead classification on a withheld test dataset was 97.3%. The accuracy of species
 380 classification on a withheld testing dataset was 66.7%. The accuracy of WPB host/non-WPB-host (i.e.,
 381 ponderosa pine versus other tree species) on a withheld testing dataset was 74.4%.

382 Site summary based on best tree detection algorithm and classification

383 Across our study site, we detected, segmented, and classified 452,413 trees (see Supplemental Table for site
 384 summaries). Estimated tree mortality at a site ranged from 6.8% to 53.6%.

385 Effect of local structure and regional climate on tree mortality attributed to western pine 386 beetle

387 We detected a small, generally positive main effect of climatic water deficit on the probability of ponderosa
 388 pine mortality within each 20 x 20-m cell (Figure 4).

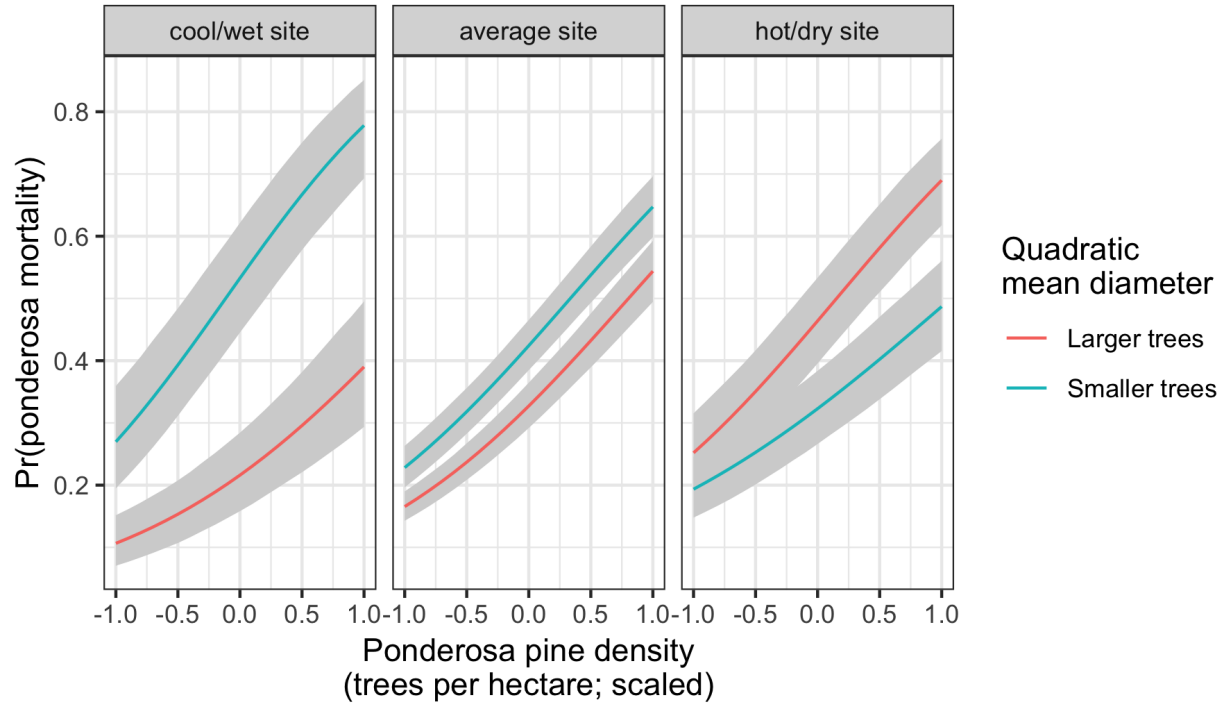


Figure 5: Line version of model results with 95% credible intervals showing primary influence of ponderosa pine structure on the probability of ponderosa pine mortality, and the interaction across climatic water deficit. The ‘larger trees’ line represents the quadratic mean diameter of ponderosa pine 0.7 standard deviations above the mean, and the ‘smaller trees’ line represents the quadratic mean diameter of ponderosa pine 0.7 standard deviations below the mean.

- 389 We found a strongly positive main effect of ponderosa pine local density, with greater density increasing the
 390 probability of ponderosa pine mortality. Conversely, we found a strong negative effect of overall tree density
 391 (i.e., including both ponderosa pine and non-host species) such that additional non-host trees in a 20 x 20-m
 392 cell (for the same number of host trees) would decrease the probability of ponderosa pine mortality (Figure
 393 4).
- 394 We found a generally negative effect of quadratic mean diameter (QMD) of ponderosa pine on the probability
 395 of ponderosa mortality, suggesting that the western pine beetle attacked smaller trees, on average. There was
 396 a strong positive interaction between the climatic water deficit and ponderosa pine QMD, such that larger
 397 trees were more likely to increase the probability of ponderosa mortality in hotter, drier sites (Figure 5).
- 398 There was a positive interaction between overall tree density and overall QMD, such that denser stands with
 399 larger trees led to greater ponderosa pine mortality, though the main effects of each of these variables were
 400 weakly negative (Figure 4).

401 **Discussion**

402 This study represents a novel use of drones to further our understanding of the simultaneous effects of local
403 forest structure and composition with broad-scale environmental gradients on tree mortality attributed to
404 WPB. We found strong positive effects (effect sizes >0.5) of both host tree density and the interaction between
405 site climatic water deficit (CWD) and host tree mean size (QMD) on the probability of ponderosa pine
406 mortality. Conversely, we found a strong negative effect (effect size <-0.5) of overall tree density. Surprisingly,
407 site CWD exerted only a weakly positive main effect on the probability of ponderosa mortality (effect size:
408 0.07; 95% CI: [-0.07, 0.20]). To that end, we did not measure tree water stress at an individual tree level as
409 in other recent work (Stephenson et al. 2019), and instead treated CWD as a general indicator of tree stress
410 following results of coarser-scale studies (Asner et al. 2016, Young et al. 2017). This may have contributed
411 to our failure to detect a stronger CWD effect. Also, our entire study area experienced the same extreme hot
412 drought between 2012 and 2015 and the variation of mortality explained by a main effect of climatic water
413 deficit may be dampened when most trees are experiencing a high degree of water stress (Floyd et al. 2009,
414 Fettig et al. 2019).

415 **Positive effect of host density and a negative effect of overall density**

416 The strongest effect on the probability of ponderosa pine mortality was the positive effect of local host density
417 within each 20 x 20-m cell (effect size: 0.91; 95% CI: [0.82, 1.00]). The relationship between host density and
418 susceptibility to colonization by bark beetles has been so well-documented at the experimental plot level (e.g.,
419 Raffa and Berryman (1987), Oliver (1995)) that lowering stand densities through selective harvest of hosts is
420 commonly recommended for reducing future levels of tree mortality attributed to bark beetles (Fettig and
421 Hilszczański 2015), including WPB (Fettig 2016). Greater host density shortens the flight distance required
422 for WPB to disperse to new host, which likely facilitates bark beetle spread, but we calibrated our aerial
423 tree detection to ~400 m² areas rather than to individual tree locations so don't have the data precision to
424 address this hypothesis directly. Increased density of ponderosa pine, specifically, may disproportionately
425 increase the competitive environment for these WPB host trees (and thus increase their susceptibility to
426 WPB colonization) if intraspecific competition amongst ponderosa pine trees is stronger than interspecific
427 competition as would be predicted with coexistence theory (Chesson 2000). Finally, greater host density
428 likely increases the frequency that WPB land on their preferred host and avoid expending energy flying to
429 non-hosts.

430 Because we also found a strong negative effect of overall tree density (host and non-host) within each cell
431 while accounting for host density (effect size: -0.80; 95% CI: [-0.89, -0.71]), we suspect that the positive

432 association between host density and host mortality is at least partially driven by mechanisms associated with
433 the relative abundance of species in a local area. That is, increasing overall tree density while keeping host
434 tree density constant (as would be the scenario to interpret the marginal negative effect of overall tree density)
435 implies an increasing proportion of non-host trees. Frequency-dependent herbivory—whereby mixed-species
436 forests experience less herbivory compared to monocultures—is common, especially for oligophagous insect
437 species (Jactel and Brockerhoff 2007). Furthermore, it has been demonstrated that nonhost volatiles reduce
438 attraction of several species of bark beetles to their aggregation pheromones (Seybold et al. 2018), including
439 WPB (Fettig et al. 2005). To that end, combinations of nonhost volatiles and an antiaggregation pheromone
440 have been used successfully to reduce levels of tree mortality attributed to WPB (e.g., Fettig et al. (2012)).
441 The negative relationship that we detected between overall tree density and host mortality corroborates
442 findings from Fettig et al. (2019), though Fettig et al. (2019) didn't simultaneously model the effect of
443 host density. In general however, Hayes et al. (2009) and Fettig et al. (2019) found that measures of host
444 availability explained less variation in mortality than measures of overall tree density, but those conclusions
445 were based on a response variable of “total number of dead host trees,” rather than the number of dead host
446 trees conditional on the total number of host trees as in our study (i.e., a binomial response).

447 **Negative main effect of host tree mean size, but strong positive interaction with site CWD**

448 Counter to our expectations, we found an overall negative effect of host tree mean size on the probability of
449 host mortality (effect size: -0.30; 95% CI: [-0.50, -0.10]). WPB exhibit a preference for trees 50.8 to 76.2 cm
450 in diameter at breast height (Person 1928, 1931), and a positive relationship between host tree size and levels
451 of tree mortality attributed to WPB was reported by Fettig et al. (2019) in the coincident field plots as well
452 as in other recent studies (Stephenson et al. 2019, Pile et al. 2019). Indeed, Fettig et al. (2019) reported no
453 mortality in ponderosa pine trees < 10.0 cm dbh. Larger trees are more nutritious and are therefore ideal
454 targets if local bark beetle density is high enough to successfully initiate mass attack as can occur when many
455 trees are under severe water stress (Bentz et al. 2010). In the recent hot drought, we expected that most trees
456 would be under severe water stress, setting the stage for increasing beetle density, successful mass attacks,
457 and targeting of larger trees. One possible explanation for our finding is that our observations represent the
458 cumulative mortality of trees during a multi-year drought event and its aftermath. Lower host tree mean size
459 led to a greater probability of host mortality earlier in the drought (Pile et al. 2019) and that signal might
460 have persisted even as mortality continued to accumulate driven by other factors. Furthermore, Fettig et
461 al. (2019) found no relationship between tree size and tree mortality for incense cedar or white fir in the
462 coincident field plots. These species represent 22.3% of the total tree mortality observed in their study, yet in
463 our study all dead trees were classified as ponderosa pine (see Methods).

464 We did observe a strong host tree size effect in its interaction with site CWD (effect size: 0.72; 95% CI: [0.37,
465 1.07]). In hot, dry sites, larger average host size increased the probability of host mortality while smaller
466 host sizes increased the probability of host mortality in cool, wet sites. This suggests that the same bark
467 beetle species was cueing into different aspects of forest structure across the environmental gradient. This
468 represents an intraspecific version of the results of Stephenson et al. (2019), who found that insect-induced
469 tree mortality in the same region during the same hot drought were driven by different factors for different
470 tree species. For instance, Stephenson et al. (2019) found that ponderosa pine mortality was largely driven
471 by host selection behavior of forest insects, where larger more nutritious trees were specifically targeted
472 regardless of whether they exhibited signs of stress. In contrast, Stephenson et al. (2019) found that white fir
473 mortality occurred predominantly in the slower growing, smaller, stressed trees. In our study, we found that,
474 even within a single pairing of forest insect species and its host, the host tree size affected host mortality
475 differently depending on the site-level climatic water deficit.

476 Despite high local levels of tree mortality across our study area (Fettig et al. 2019), our results from surveying
477 the broader context surrounding coincident field plots reveals different effects of host tree size depending
478 on CWD, and perhaps different stages of bark beetle disturbance across the environmental gradient. For
479 primary bark beetles, massive tree mortality as observed from the 2012-2015 drought and its aftermath does
480 not necessarily distinguish “endemic” from “outbreak” phases of bark beetle disturbance, which is instead
481 distinguished by the underlying driver of bark beetle host selection behavior (Logan et al. 1998). “Endemic”
482 phases are distinguished by environmental determinism, when beetles select hosts based on whether they are
483 weakened in some way, often by environmental conditions. “Outbreak” phases are distinguished by dynamic
484 determinism, when population dynamics reign— when local beetle density is high enough that intraspecific
485 pheromone communication dominates host selection, successful mass attacks are likely, and even large healthy
486 trees can be killed (White and Powell 1997, Logan et al. 1998). Different outbreak cycle phases may help
487 explain the especially high host mortality in high host density, low host size cells that we observed in cool/wet
488 sites (Figure 5). The smaller trees would presumably be nutritionally sub-optimal, and thus unexpected
489 targets if the WPB were indeed in an “outbreak” phase at these sites and able to attack even large, healthy
490 trees. While trees were likely water stressed across the whole study due to the extreme drought, we expected
491 generally less water stress in the cool/wet sites, and generally higher water stress in the hot/dry sites (Asner
492 et al. 2016, Young et al. 2017). Thus, it is possible that the observed mortality patterns across the Sierra
493 Nevada during the 2012-2015 hot drought arose as synergistic alignment of environmental conditions and
494 complex forest structure enabled the WPB to cross thresholds of “outbreak” behavior in the hottest, driest
495 sites but such an alignment was not present in the cooler, wetter sites (Raffa et al. 2008).

496 **Limitations and future directions**

497 We have demonstrated that drones can be effective means of collecting forest data at multiple, vastly different
498 spatial scales to investigate a single, multi-scale phenomenon— from meters in between trees, to hundreds
499 of meters of elevation, to hundreds of thousands of meters of latitude. Some limitations remain but can be
500 overcome with further refinements in the use of this tool for forest ecology. Most of these limitations arise
501 from tree detection and classification uncertainty, and thus it was imperative to work with field data for
502 calibration and uncertainty reporting.

503 The greatest limitation in our study arising from classification uncertainty is in the assumption that all
504 dead trees were ponderosa pine. While spectral information of foliage could help classify living trees to
505 species, standing dead trees did not reflect differently for different species. We estimate from coincident field
506 plots that this is true approximately 73.4% of the time. Because tree mortality response to forest insects is
507 species-specific, even with sympatric tree species during the same hot drought (Stephenson et al. 2019), we
508 cannot entirely rule out that some of the mortality responses to complex forest structure that we observed
509 arose from these species-specific responses. The overall community composition across our study area was not
510 very different (Fettig et al. 2019), so we remain confident that the patterns we observed were driven primarily
511 by the dynamic between the western pine beetle and ponderosa pine. This challenge of classifying standing
512 dead trees to species implies that a conifer forest system with less bark beetle and tree host diversity, such as
513 mountain pine beetle-induced mortality in monocultures of lodgepole pine, should be particularly amenable
514 to the methods presented here even with minimal further refinement because a dead tree will almost certainly
515 belong to a single species and have succumbed due to bark beetle colonization.

516 Some uncertainty surrounded our ability to detect trees using the geometry of the dense point clouds derived
517 with SfM. The horizontal accuracy of the tree detection was better than the vertical accuracy, which may
518 result from a more significant error contribution by the field-based calculations of tree height compared to
519 tree position relative to plot center (Table 2). Both the horizontal and vertical accuracy would likely improve
520 with better SfM point clouds, which requires imagery with more overlap. Frey et al. (2018) recently found
521 that 95% overlap was preferable for generating dense point clouds, and we only achieved 91.6% overlap with
522 the X3 RGB camera and 83.9% overlap with the multispectral camera. While our live/dead classification was
523 fairly accurate (97.3% on a withheld dataset), our species classifier would likely benefit from better crown
524 segmentation because the pixel-level reflectance values within each crown are averaged to characterize the
525 “spectral signature” of each tree. With better delineation of each tree crown, the mean value of pixels within
526 each tree crown will likely be more representative of that tree’s spectral signature. Better crown segmentation
527 would most readily be achieved through greater overlap in imagery. Finally, we anticipate that computer

528 vision and deep learning will prove helpful in overcoming some of these detection and classification challenges
529 (Gray et al. 2019).

530 **Conclusions**

531 Climate change adaptation strategies emphasize reducing tree densities to restore forest resilience (North et
532 al. 2015, Young et al. 2017), but understanding the optimal complex forest structure that can enable dry
533 western U.S. forests to persist through disturbances such as insect attack will be vital for predicting how
534 California forests may respond to these interventions. We've shown that drones can be a valuable tool for
535 investigating how this complexity in forest structure combines with environmental conditions to shape forest
536 insect disturbance.

537 Our results support conclusions of other researchers that management interventions to reduce the severity of
538 bark beetle disturbance will benefit from generally reducing host density (Young et al. 2017). In addition
539 however, our study suggests that outcomes will depend on whether the disturbance dynamic has crossed
540 endemic to outbreak feedback thresholds (Raffa et al. 2008), which may be predicted by recent advances in
541 disturbance forecasting (Preisler et al. 2017).

542 **Acknowledgements**

543 We gratefully acknowledge funding from the USDA Forest Service Western Wildlands Environmental Threat
544 Assessment Center (WWETAC) and the Pacific Southwest Research Station Climate Change Competitive
545 Grant Program. We thank Connie Millar for comments and guidance during the development of this project
546 and Victoria Scholl for helpful discussions regarding remotely sensed data product levels.

547 **References**

- 548 Anderegg, W. R. L., J. A. Hicke, R. A. Fisher, C. D. Allen, J. Aukema, B. Bentz, S. Hood, J. W. Lichstein,
549 A. K. Macalady, N. McDowell, Y. Pan, K. Raffa, A. Sala, J. D. Shaw, N. L. Stephenson, C. Tague, and
550 M. Zeppel. 2015. Tree mortality from drought, insects, and their interactions in a changing climate. *New*
551 *Phytologist* 208:674–683.
- 552 Asner, G. P., P. G. Brodrick, C. B. Anderson, N. Vaughn, D. E. Knapp, and R. E. Martin. 2016. Progressive
553 forest canopy water loss during the 2012–2015 California drought. *Proceedings of the National Academy of*
554 *Sciences* 113:E249–E255.
- 555 Baldwin, B. G., A. H. Thornhill, W. A. Freyman, D. D. Ackerly, M. M. Kling, N. Morueta-Holme, and B. D.

- 556 Mishler. 2017. Species richness and endemism in the native flora of California. American Journal of Botany
557 104:487–501.
- 558 Bedard, W. D., P. E. Tilden, D. L. Wood, R. M. Silverstein, R. G. Brownlee, and J. O. Rodin. 1969.
559 Western pine beetle: Field response to its sex pheromone and a synergistic host terpene, myrcene. Science
560 164:1284–1285.
- 561 Bentz, B. J., J. Régnière, C. J. Fettig, E. M. Hansen, J. L. Hayes, J. A. Hicke, R. G. Kelsey, J. F. Negrón,
562 and S. J. Seybold. 2010. Climate change and bark beetles of the western United States and Canada: Direct
563 and indirect effects. BioScience 60:602–613.
- 564 Berryman, A. A. 1982. Population dynamics of bark beetles. Pages 264–314 in Bark Beetles in North
565 American Conifers: A System for the Study of Evolutionary Biology.
- 566 Brooks, S. P., and A. Gelman. 1998. General methods for monitoring convergence of iterative simulations.
567 Journal of Computational and Graphical Statistics 7:434.
- 568 Bürkner, P.-C. 2017. **brms**: An *R* package for bayesian multilevel models using *Stan*. Journal of Statistical
569 Software 80.
- 570 Byers, J. A., and D. L. Wood. 1980. Interspecific inhibition of the response of the bark beetles, *Dendroctonus*
571 *brevicomis* and *Ips paraconfusus*, to their pheromones in the field. Journal of Chemical Ecology 6:149–164.
- 572 Chesson, P. 2000. Mechanisms of Maintenance of Species Diversity. Annual Review of Ecology and Systematics
573 31:343–366.
- 574 Chubaty, A. M., B. D. Roitberg, and C. Li. 2009. A dynamic host selection model for mountain pine beetle,
575 *Dendroctonus ponderosae* Hopkins. Ecological Modelling 220:1241–1250.
- 576 Clevers, J., and A. Gitelson. 2013. Remote estimation of crop and grass chlorophyll and nitrogen content using
577 red-edge bands on Sentinel-2 and -3. International Journal of Applied Earth Observation and Geoinformation
578 23:344–351.
- 579 Coops, N. C., M. Johnson, M. A. Wulder, and J. C. White. 2006. Assessment of QuickBird high spatial
580 resolution imagery to detect red attack damage due to mountain pine beetle infestation. Remote Sensing of
581 Environment 103:67–80.
- 582 DJI. 2015a. Zenmuse X3 - Creativity Unleashed. <https://www.dji.com/zenmuse-x3/info>.
- 583 DJI. 2015b. DJI - The World Leader in Camera Drones/Quadcopters for Aerial Photography. <https://www.dji.com/matrice100/info>.

- 585 DronesMadeEasy. 2018. Map Pilot for DJI on iOS. [https://itunes.apple.com/us/app/map-pilot-for-dji/
586 id1014765000?mt=8](https://itunes.apple.com/us/app/map-pilot-for-dji/id1014765000?mt=8).
- 587 Evenden, M. L., C. M. Whitehouse, and J. Sykes. 2014. Factors influencing flight capacity of the mountain
588 pine beetle (Coleoptera: Curculionidae: Scolytinae). *Environmental Entomology* 43:187–196.
- 589 Eysn, L., M. Hollaus, E. Lindberg, F. Berger, J.-M. Monnet, M. Dalponte, M. Kobal, M. Pellegrini, E.
590 Lingua, D. Mongus, and N. Pfeifer. 2015. A benchmark of LiDAR-based single tree detection methods using
591 heterogeneous forest data from the alpine space. *Forests* 6:1721–1747.
- 592 Farr, T. G., P. A. Rosen, E. Caro, R. Crippen, R. Duren, S. Hensley, M. Kobrick, M. Paller, E. Rodriguez, L.
593 Roth, D. Seal, S. Shaffer, J. Shimada, J. Umland, M. Werner, M. Oskin, D. Burbank, and D. Alsdorf. 2007.
594 The Shuttle Radar Topography Mission. *Reviews of Geophysics* 45.
- 595 Fettig, C. J. 2012. Chapter 2: Forest health and bark beetles. *in* Managing Sierra Nevada Forests. PSW-
596 GTR-237. USDA Forest Service.
- 597 Fettig, C. J. 2016. Native bark beetles and wood borers in Mediterranean forests of California. Pages 499–528
598 *in* Insects and diseases of Mediterranean Forest systems. Springer International Publishing, Switzerland.
- 599 Fettig, C. J., and J. Hilszczański. 2015. Management strategies for bark beetles in conifer forests. Pages
600 555–584 *in* Bark Beetles. Elsevier.
- 601 Fettig, C. J., K. D. Klepzig, R. F. Billings, A. S. Munson, T. E. Nebeker, J. F. Negrón, and J. T. Nowak. 2007.
602 The effectiveness of vegetation management practices for prevention and control of bark beetle infestations in
603 coniferous forests of the western and southern United States. *Forest Ecology and Management* 238:24–53.
- 604 Fettig, C. J., S. R. McKelvey, C. P. Dabney, D. P. W. Huber, C. G. Lait, D. L. Fowler, and J. H. Borden. 2012.
605 Efficacy of “Verbenone Plus” for protecting ponderosa pine trees and stands from *Dendroctonus brevicomis*
606 (Coleoptera: Curculionidae) attack in British Columbia and California. *Journal of Economic Entomology*
607 105:1668–1680.
- 608 Fettig, C. J., S. R. McKelvey, and D. P. W. Huber. 2005. Nonhost angiosperm volatiles and Verbenone disrupt
609 response of western pine beetle, *Dendroctonus brevicomis* (Coleoptera: Scolytidae), to attractant-baited traps.
610 *Journal of Economic Entomology* 98:2041–2048.
- 611 Fettig, C. J., L. A. Mortenson, B. M. Bulaon, and P. B. Foulk. 2019. Tree mortality following drought in the
612 central and southern Sierra Nevada, California, U.S. *Forest Ecology and Management* 432:164–178.
- 613 Flint, L. E., A. L. Flint, J. H. Thorne, and R. Boynton. 2013. Fine-scale hydrologic modeling for regional land-

- 614 scape applications: The California Basin Characterization Model development and performance. Ecological
615 Processes 2:25.
- 616 Floyd, M. L., M. Clifford, N. S. Cobb, D. Hanna, R. Delph, P. Ford, and D. Turner. 2009. Relationship of
617 stand characteristics to drought-induced mortality in three Southwestern piñonJuniper woodlands. Ecological
618 Applications 19:1223–1230.
- 619 Franceschi, V. R., P. Krokene, E. Christiansen, and T. Krekling. 2005. Anatomical and chemical defenses of
620 conifer bark against bark beetles and other pests. New Phytologist 167:353–376.
- 621 Frey, J., K. Kovach, S. Stemmler, and B. Koch. 2018. UAV photogrammetry of forests as a vulnerable
622 process. A sensitivity analysis for a structure from motion RGB-image pipeline. Remote Sensing 10:912.
- 623 Gabry, J., D. Simpson, A. Vehtari, M. Betancourt, and A. Gelman. 2019. Visualization in Bayesian workflow.
624 Journal of the Royal Statistical Society: Series A (Statistics in Society) 182:389–402.
- 625 Gitelson, A., and M. N. Merzlyak. 1994. Spectral reflectance changes associated with autumn senescence of
626 *Aesculus hippocastanum* L. And *Acer platanoides* L. Leaves. Spectral features and relation to chlorophyll
627 estimation. Journal of Plant Physiology 143:286–292.
- 628 Graf, M., M. Reid, B. Aukema, and B. Lindgren. 2012. Association of tree diameter with body size and lipid
629 content of mountain pine beetles. The Canadian Entomologist 144:467–477.
- 630 Gray, P. C., A. B. Fleishman, D. J. Klein, M. W. McKown, V. S. Bézy, K. J. Lohmann, and D. W. Johnston.
631 2019. A convolutional neural network for detecting sea turtles in drone imagery. Methods in Ecology and
632 Evolution 10:345–355.
- 633 Griffin, D., and K. J. Anchukaitis. 2014. How unusual is the 2012-2014 California drought? Geophysical
634 Research Letters 41:9017–9023.
- 635 Hayes, C. J., C. J. Fettig, and L. D. Merrill. 2009. Evaluation of multiple funnel traps and stand characteristics
636 for estimating western pine beetle-caused tree mortality. Journal of Economic Entomology 102:2170–2182.
- 637 Hijmans, R. J., J. van Etten, M. Sumner, J. Cheng, A. Bevan, R. Bivand, L. Busetto, M. Canty, D. Forrest,
638 A. Ghosh, D. Golicher, J. Gray, J. A. Greenberg, P. Hiemstra, I. for M. A. Geosciences, C. Karney, M.
639 Mattiuzzi, S. Mosher, J. Nowosad, E. Pebesma, O. P. Lamigueiro, E. B. Racine, B. Rowlingson, A. Shortridge,
640 B. Venables, and R. Wueest. 2019. Raster: Geographic data analysis and modeling.
- 641 Hunziker, P. 2017. Velox: Fast raster manipulation and extraction.
- 642 Jactel, H., and E. G. Brockerhoff. 2007. Tree diversity reduces herbivory by forest insects. Ecology Letters

643 10:835–848.

644 Jakubowski, M. K., W. Li, Q. Guo, and M. Kelly. 2013. Delineating individual trees from LiDAR data: A
645 comparison of vector- and raster-based segmentation approaches. *Remote Sensing* 5:4163–4186.

646 Kane, V. R., M. P. North, J. A. Lutz, D. J. Churchill, S. L. Roberts, D. F. Smith, R. J. McGaughey, J. T.
647 Kane, and M. L. Brooks. 2014. Assessing fire effects on forest spatial structure using a fusion of Landsat and
648 airborne LiDAR data in Yosemite National Park. *Remote Sensing of Environment* 151:89–101.

649 Kolb, T. E., C. J. Fettig, M. P. Ayres, B. J. Bentz, J. A. Hicke, R. Mathiasen, J. E. Stewart, and A. S. Weed.
650 2016. Observed and anticipated impacts of drought on forest insects and diseases in the United States. *Forest
651 Ecology and Management* 380:321–334.

652 Kuhn, M. 2008. Building predictive models in R using the caret package. *Journal of Statistical Software*
653 28:1–26.

654 Larson, A. J., and D. Churchill. 2012. Tree spatial patterns in fire-frequent forests of western North America,
655 including mechanisms of pattern formation and implications for designing fuel reduction and restoration
656 treatments. *Forest Ecology and Management* 267:74–92.

657 Li, W., Q. Guo, M. K. Jakubowski, and M. Kelly. 2012. A new method for segmenting individual trees from
658 the LiDAR point cloud. *Photogrammetric Engineering & Remote Sensing* 78:75–84.

659 Logan, J. A., P. White, B. J. Bentz, and J. A. Powell. 1998. Model analysis of spatial patterns in mountain
660 pine beetle outbreaks. *Theoretical Population Biology* 53:236–255.

661 Meyer, F., and S. Beucher. 1990. Morphological segmentation. *Journal of Visual Communication and Image
662 Representation* 1:21–46.

663 Micasense. 2015. MicaSense. <https://support.micasense.com/hc/en-us/articles/215261448-RedEdge-User-Manual-PDF-Downl>

664 Millar, C. I., R. D. Westfall, D. L. Delany, M. J. Bokach, A. L. Flint, and L. E. Flint. 2012. Forest mortality in
665 high-elevation whitebark pine (*Pinus albicaulis*) forests of eastern California, USA: Influence of environmental
666 context, bark beetles, climatic water deficit, and warming. *Canadian Journal of Forest Research* 42:749–765.

667 Miller, J. M., and F. P. Keen. 1960. Biology and control of the western pine beetle: A summary of the first
668 fifty years of research. US Department of Agriculture.

669 Moeck, H. A., D. L. Wood, and K. Q. Lindahl. 1981. Host selection behavior of bark beetles (Coleoptera:
670 Scolytidae) attacking *Pinus ponderosa*, with special emphasis on the western pine beetle, *Dendroctonus
671 brevicomis*. *Journal of Chemical Ecology* 7:49–83.

- 672 Morris, J. L., S. Cottrell, C. J. Fettig, W. D. Hansen, R. L. Sherriff, V. A. Carter, J. L. Clear, J. Clement, R.
673 J. DeRose, J. A. Hicke, P. E. Higuera, K. M. Mattor, A. W. R. Seddon, H. T. Seppä, J. D. Stednick, and S.
674 J. Seybold. 2017. Managing bark beetle impacts on ecosystems and society: Priority questions to motivate
675 future research. *Journal of Applied Ecology* 54:750–760.
- 676 North, M. P., S. L. Stephens, B. M. Collins, J. K. Agee, G. Aplet, J. F. Franklin, and P. Z. Fule. 2015.
677 Reform forest fire management. *Science* 349:1280–1281.
- 678 Oliver, W. W. 1995. Is self-thinning in ponderosa pine ruled by *Dendroctonus* bark beetles? Page 6 *in* Forest
679 health through silviculture: Proceedings of the 1995 National Silviculture Workshop.
- 680 Pau, G., F. Fuchs, O. Sklyar, M. Boutros, and W. Huber. 2010. EBImage: An R package for image processing
681 with applications to cellular phenotypes. *Bioinformatics* 26:979–981.
- 682 Person, H. L. 1928. Tree selection by the western pine beetle. *Journal of Forestry* 26:564–578.
- 683 Person, H. L. 1931. Theory in explanation of the selection of certain trees by the western pine beetle. *Journal
684 of Forestry* 29:696–699.
- 685 Pile, L. S., M. D. Meyer, R. Rojas, O. Roe, and M. T. Smith. 2019. Drought impacts and compounding
686 mortality on forest trees in the southern Sierra Nevada. *Forests* 10:237.
- 687 Plowright, A. 2018. ForestTools: Analyzing remotely sensed forest data.
- 688 Preisler, H. K., N. E. Grulke, Z. Heath, and S. L. Smith. 2017. Analysis and out-year forecast of beetle,
689 borer, and drought-induced tree mortality in California. *Forest Ecology and Management*. 399: 166-178
690 399:166–178.
- 691 Raffa, K. F., B. H. Aukema, B. J. Bentz, A. L. Carroll, J. A. Hicke, M. G. Turner, and W. H. Romme. 2008.
692 Cross-scale drivers of natural disturbances prone to anthropogenic amplification: The dynamics of bark beetle
693 eruptions. *BioScience* 58:501–517.
- 694 Raffa, K. F., and A. A. Berryman. 1983. The role of host plant resistance in the colonization behavior and
695 ecology of bark beetles (Coleoptera: Scolytidae). *Ecological Monographs* 53:27–49.
- 696 Raffa, K. F., and A. A. Berryman. 1987. Interacting selective pressures in conifer-bark beetle systems: A
697 basis for reciprocal adaptations? *The American Naturalist* 129:234–262.
- 698 Raffa, K. F., J.-C. Grégoire, and B. Staffan Lindgren. 2015. Natural history and ecology of bark beetles.
699 Pages 1–40 *in* Bark Beetles. Elsevier.

- 700 R Core Team. 2018. R: A language and environment for statistical computing. R Foundation for Statistical
701 Computing, Vienna, Austria.
- 702 Rouse, W., R. H. Haas, W. Deering, and J. A. Schell. 1973. Monitoring the vernal advancement and
703 retrogradation (green wave effect) of natural vegetation. Type II Report, Goddard Space Flight Center,
704 Greenbelt, MD, USA.
- 705 Roussel, J.-R. 2019. lidRplugins: Extra functions and algorithms for lidR package.
- 706 Roussel, J.-R., D. Auty, F. De Boissieu, and A. S. Meador. 2019. lidR: Airborne LiDAR data manipulation
707 and visualization for forestry applications.
- 708 Seidl, R., J. Müller, T. Hothorn, C. Bässler, M. Heurich, and M. Kautz. 2016. Small beetle, large-scale
709 drivers: How regional and landscape factors affect outbreaks of the European spruce bark beetle. *The Journal*
710 of applied ecology 53:530–540.
- 711 Seybold, S. J., B. J. Bentz, C. J. Fettig, J. E. Lundquist, R. A. Progar, and N. E. Gillette. 2018. Management
712 of western North American bark beetles with semiochemicals. *Annual Review of Entomology* 63:407–432.
- 713 Shepherd, W. P., D. P. W. Huber, S. J. Seybold, and C. J. Fettig. 2007. Antennal responses of the western
714 pine beetle, *Dendroctonus brevicomis* (Coleoptera: Curculionidae), to stem volatiles of its primary host,
715 *Pinus ponderosa*, and nine sympatric nonhost angiosperms and conifers. *Chemoecology* 17:209–221.
- 716 Shiklomanov, A. N., B. A. Bradley, K. M. Dahlin, A. M. Fox, C. M. Gough, F. M. Hoffman, E. M. Middleton,
717 S. P. Serbin, L. Smallman, and W. K. Smith. 2019. Enhancing global change experiments through integration
718 of remote-sensing techniques. *Frontiers in Ecology and the Environment* 0.
- 719 Shin, P., T. Sankey, M. Moore, and A. Thode. 2018. Evaluating unmanned aerial vehicle images for estimating
720 forest canopy fuels in a ponderosa pine stand. *Remote Sensing* 10:1266.
- 721 Stephenson, N. 1998. Actual evapotranspiration and deficit: Biologically meaningful correlates of vegetation
722 distribution across spatial scales. *Journal of Biogeography* 25:855–870.
- 723 Stephenson, N. L., A. J. Das, N. J. Ampersee, and B. M. Bulaon. 2019. Which trees die during drought?
724 The key role of insect host-tree selection. *Journal of Ecology*:75.
- 725 Thistle, H. W., H. Peterson, G. Allwine, B. Lamb, T. Strand, E. H. Holsten, and P. J. Shea. 2004. Surrogate
726 pheromone plumes in three forest trunk spaces: Composite statistics and case studies. *Forest Science* 50.
- 727 USDAFS. 2019, February 11. Press Release: Survey finds 18 million trees died in California in 2018.
728 https://www.fs.usda.gov/Internet/FSE_DOCUMENTS/FSEPRD609321.pdf.

- 729 Vega, C., A. Hamrouni, S. El Mokhtari, J. Morel, J. Bock, J. P. Renaud, M. Bouvier, and S. Durrieu. 2014.
- 730 PTrees: A point-based approach to forest tree extraction from LiDAR data. International Journal of Applied
- 731 Earth Observation and Geoinformation 33:98–108.
- 732 White, P., and J. Powell. 1997. Phase transition from environmental to dynamic determinism in mountain
- 733 pine beetle attack. Bulletin of Mathematical Biology 59:609–643.
- 734 Wyngaard, J., L. Barbieri, A. Thomer, J. Adams, D. Sullivan, C. Crosby, C. Parr, J. Klump, S. Raj Shrestha,
- 735 and T. Bell. 2019. Emergent challenges for science sUAS data management: Fairness through community
- 736 engagement and best practices development. Remote Sensing 11:1797.
- 737 Young, D. J. N., J. T. Stevens, J. M. Earles, J. Moore, A. Ellis, A. L. Jirka, and A. M. Latimer. 2017.
- 738 Long-term climate and competition explain forest mortality patterns under extreme drought. Ecology Letters
- 739 20:78–86.
- 740 Zhang, W., J. Qi, P. Wan, H. Wang, D. Xie, X. Wang, and G. Yan. 2016. An easy-to-use airborne LiDAR
- 741 data filtering method based on cloth simulation. Remote Sensing 8:501.